Journal of
Information Systems Engineering
and Business Intelligence

Vol.8, No.2, October 2022
Available online at: http://e-journal.unair.ac.id/index.php/JISEBI

Chest X-ray Image Classification for COVID-19 diagnoses

Endra Yuliawan[1)*], Shofwatul 'Uyun[2)]

[1)2)] *Department of Informatics, Faculty of Science and Technology, Universitas Islam Negeri Sunan Kalijaga Yogyakarta, Indonesia*

Laksda Adisucipto Street, Papringan, Caturtunggal, District. Depok, Sleman, Daerah Istimewa Yogyakarta

[1)]indrajho168@gmail.com, [2)]shofwatul.uyun@uin-suka.ac.id

Abstract

Background: Radiologists used chest radiographs to detect coronavirus disease 2019 (COVID-19) in patients and determine the severity levels. The COVID-19 cases were grouped into five classes, each receiving different treatments. An intelligent system is needed to advance the detection and identify vector features of X-ray images with a quality that is too poor to be read by radiologists. Deep learning is an intelligent system that can be used in this case.
Objective: The current study compares the classification and accuracy of detection methods with two, three dan five classes.
Methods: Deep learning can classify visual geometry group VGG 19 architectures with 1000 classes. The classification of the five classes' convolutional neural network (CNN) underwent model validation with a confusion matrix to produce accuracy and class values. The system could then diagnose patients' examinations by radiology specialists.
Results: The results of the five-class method showed 98% accuracy, the three-class method showed 99.99%, and the two-class showed 99.99%.
Conclusion: It can be concluded that using the VGG 19 model is effective. This system can classify and diagnose viruses in patients to assist radiologists by reading the images.

Keywords*:* COVID-19, CNN, Classification, Deep Learning

Article history*:* Received 1 August 2022, first decision 22 August 2022, accepted 8 September 2022, available online 28 October 2022

I. INTRODUCTION

The SARS-CoV2, a coronavirus with a crown-like structure, is highly transmittable [1], with a case fatality rate of 2%. Severe cases may lead to alveolar destruction, progressive respiratory failure, and eventually death [2]. Early diagnostics will benefit patients because appropriate treatment can be given immediately. Radiologists can do this by examining chest X-rays. However, a limited number of hospital radiologists may not handle the high demand for chest X-ray readings. Therefore, automatization is needed to provide timely referrals for quarantine or further monitoring.

Incubation of COVID-19 is five or six days, but it can also be up to 14 days.[3, 4]. Transmissions can occur through droplets from patients when talking, coughing or sneezing [5]. Droplets generally have a diameter of >5-10 μm, with those having a diameter of 5 μm considered easily transmitted aerosol. Close contact at a one-metre distance with an infected person [6] can quickly spread the virus. In this study, we examine chest X-ray images to determine whether the lungs are infected with the COVID-19 virus or pneumonia based on the morphology. A second reader assists a radiology doctor in using these results to guide intelligent computational categorisation. A clinical image reader oversees the process. The researcher focuses on radiographic images despite other images such as MRI, tomography, etc.

The development of artificial intelligence (AI) has been implemented in many sectors, including medical sciences. An example is the improvement of devices to assist in treatments or diagnoses of chronic and non-chronic diseases. An intelligent computational approach can assist clinicians by simplifying the process and treating patients efficiently. The intelligent system in this study is a chest thorax photo reader, which is processed through an in-depth learning model, and displays accurate results of COVID-19 diagnoses.

We implemented this study's convolutional neural network (CNN) to predict COVID-19 cases using the VGG 19 architectural model. We used chest thoracic images generated by experts or radiologists (public datasets). Dynamic CNN (DCNN) is a learning algorithm widely used for practical applications, such as computerised vision tasks, shape pattern detection, and image classification. These applications have significantly helped decision-making in different

* Corresponding author

ISSN 2443-2555 (online) 2598-6333 (print)
doi: http://dx.doi.org/10.20473/jisebi.8.2.109-118

contexts [7]. In the health sector, studies on this topic have been extensive, especially concerning COVID-19. Our study proposes different methods for detecting and classifying chest X-ray images. Apostolopoulos [2] uses a CNN algorithm with visual geometry group (VGG) 19 architecture to classify three and two classes (COVID+, Normal and Pneumonia). Priyansh Kedia [17], with the proposed CoVNet-19 model, uses VGG 19, DenseNet-121 and SVM architectures to classify three and two classes (COVID+, Normal and Pneumonia). Hemdan [9] uses VGG 19 to classify two classes (COVID+ and COVID-). Gour [10] proposed the StakedCNN model to classify three and two classes (COVID-19, Normal and Pneumonia). Shelke [11] proposed the VGG16, DenseNet-161 and Resnet-18 models to classify four classes (Pneumonia, COVID-19, Normal and Tuberculosis). E.Hussian [12] proposed the Corodet model to classify four, three and twso classes (COVID-19, Normal, viral pneumonia and bacterial pneumonia).

This study aims to see the severity of each patient infected with the COVID-19 virus. Specifically, this study analyses and compares the level of accuracy of each class on the CNN model with the VGG 19 architecture on the X-ray photos to: 1) construct a new model, 2) measure the model's accuracy, 3) propose five new classes (Mild COVID, Severe COVID, Normal, Mild Pneumonia, Severe Pneumonia).

II. METHODS

This section describes the dataset and the proposed method, i.e., pre-processing, training, classification, convolution neural network, and visual geometry group network 19, as shown in Fig. 1. The output of the CNN deep learning process with the VGG 19 architecture was tested through class validation and the confusion matrix. Data were obtained via public datasets GitHub and Kaggle [14][8].

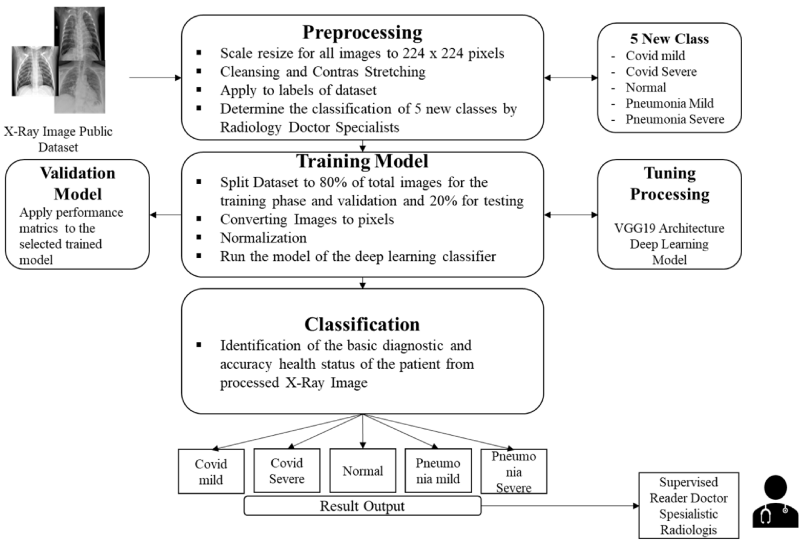

Fig. 1 Proposed Method Classification

In the pre-processing stage, the chest X-ray images are resized to 224x224 pixels. Next, the images are cleansed, and the contrast is stretched to enhance the sharpness and clarity. The output of this stage is readable textures or shapes. Then, the dataset is labelled and grouped into five classes: Mild COVID, Severe COVID, COVID Normal, Mild Pneumonia, and Severe Pneumonia by radiology specialists. The model allocates 80% of the data for training and validation and 20% for testing. The conversion of chest X-ray images results in an array value convertible to a binary system with the numbers 0 and 1. The array of values was then normalised, and the proposed deep learning model was run for classification. The model validation is done through a matrix that displays the model performance. The next stage is to identify the disease class and assess the accuracy value of the classification results. Radiology specialists then corroborate the results to check the model's accuracy.

A. Dataset

The data used in this study were taken from chest radiograph public databases, i.e., Kaggle and GitHub [9,10], which were then pre-processed with revalidated. The number of images readable by radiologists was 2350. The classification resulted in 470 Severe COVID, 470 Mild COVID, 470 Normal, 470 Severe Pneumonia, and 470 Mild Pneumonia in

jpg format dimensions of 224x224 pixels. Fig. 2 is an example of the classified chest radiograph/thorax image, and Table 1 is a distribution of data from Kaggle (Kermany, [10]; CoroNet, [9]).

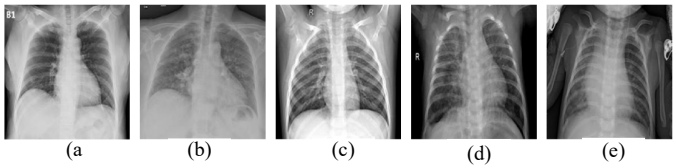

(a) (b) (c) (d) (e)

Fig. 2 Thorax Image example (a) Mild COVID; (b) Severe COVID; (c) COVID Normal; (d) Mild Pneumonia; (e) Severe Pneumonia

TABLE 1
IMAGE DISTRIBUTION DATASET

Dataset	Reference	Covid Mild	Covid Severe	Normal	Pneumonia Mild	Pneumonia severe
1	Kaggle(kermany)	200	270	470	0	250
2	Github(CoroNet)	270	200	0	470	220
	Total	**470**	**470**	**470**	**470**	**470**

B. Pre-Processing

In Fig. 2, the initial stage before testing, the data were adjusted to be processed with a size scaling of 224x224 pixels. Then, the dataset was cleansed for radiologists so that they could classify them. Then, the contrast stretching was done by (1) to sharpen the image's colour, as shown in Fig. 3.

$$o(i,j) = \frac{u(i,j)-c}{d-c}(L-1) \tag{1}$$

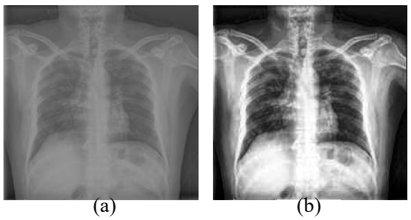

(a) (b)

Fig. 3 Example of thorax images from contrast stretching (a) before pre-processing; (b) after pre-processing.

In Equation (1), *o(i,j)* and *u(i,j)*) are pixels after and before being transformed in *(i,j)* coordinates, while *c* and *d* respectively represent the maximum and minimum values of pixels in the input image, and L represents the maximum grayscale value. If the pixel value is smaller than 0, then it will be made 0, and if it is greater than *(L-1),* it will be used as *(L-1)* [11]. The contrast stretching enhanced the quality of the images. Then, the labelling of the thorax image data by radiology specialists showed the classes were Mild COVID, Severe COVID, COVID Normal, Mild Pneumonia, and Severe Pneumonia. The chest radiographs were grouped according to the proposed five classes.

C. Training Model

At this stage, the dataset was divided into 80% for training and validation and 20% for testing. Next, the images were converted into pixel values and normalised into binary values. Finally, data were classified using the VGG 19 architecture and validated using a matrix.

D. Classification

The next stage is the grouping into five classes: Mild COVID, Severe COVID, COVID Normal, Mild Pneumonia, and Severe Pneumonia, using the VGG 19 architecture. The radiologists then corroborated the output results.

CNN is an algorithm with a neuron structure that interprets the input data (X_1), combining them with a constant weight (W_1). The weight compresses the input according to its relevance, and the results are passed through a non-linear activation function $F(\sum W_i X)_i$ as seen on Fig. 4. These neurons are stacked together to create a layer of the network. Three or more layers create deep neural networks (DNN). The network calculates advanced features and high-level trends in a large dimensional and non-linear data series. The results were then used to create classification

and grouping of data. The optimal weight matrix of neurons was calculated using an optimisation procedure. The loss function was minimised by considering the input data points.

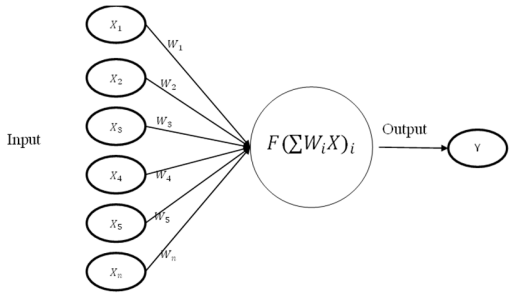

Fig. 4. Building block of the neural network

E. Visual Geometry Group Network 19

The CNN architecture, runner-up at ILSVRC 2014 [12], has 16 convolution layers. Five max-pooling reduces image resolution, commonly used in CNN models [13,14]. Three full connected layers and one softmax are shown in Fig. 5.

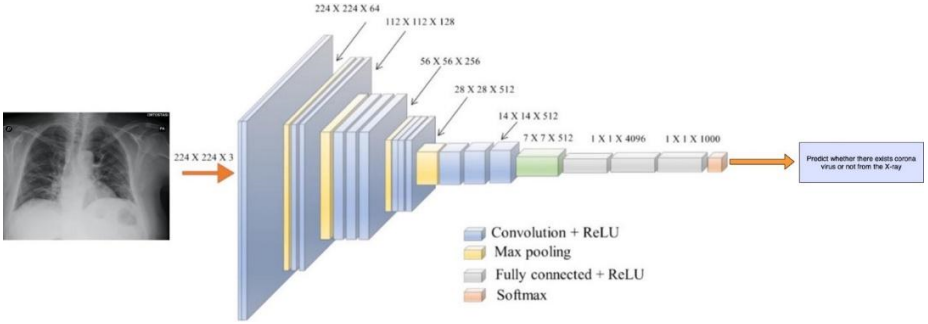

Fig. 5. The VGG 19 architecture

TABLE 2
SUMMARY ON VGG 19 LAYERS MODEL

Layer	Output Shape	Parameter
block1_conv1 (Conv2D)	(224, 224, 64)	1792
block1_conv2 (Conv2D)	(224, 224, 64)	36928
block1_pool (MaxPooling2D)	(112, 112, 64)	0
block2_conv1 (Conv2D)	(112, 112, 128)	73856
block2_conv2 (Conv2D)	(112, 112, 128)	147584
block2_pool (MaxPooling2D)	(56, 56, 128)	0
block3_conv1 (Conv2D)	(56, 56, 256)	295168
block3_conv2 (Conv2D)	(56, 56, 256)	590080
block3_conv3 (Conv2D)	(56, 56, 256)	590080
block3_conv4 (Conv2D)	(56, 56, 256)	590080
block3_pool (MaxPooling2D)	(28, 28, 256)	0
block4_conv1 (Conv2D)	(28, 28, 512)	1180160
block4_conv2 (Conv2D)	(28, 28, 512)	2359808
block4_conv3 (Conv2D)	(28, 28, 512)	2359808
block4_conv4 (Conv2D)	(28, 28, 512)	2359808
block4_pool (MaxPooling2D)	(14, 14, 512)	0
block5_conv1 (Conv2D)	(14, 14, 512)	2359808
block5_conv2 (Conv2D)	(14, 14, 512)	2359808
block5_conv3 (Conv2D)	(14, 14, 512)	2359808
block5_conv4 (Conv2D)	(14, 14, 512)	2359808
block5_pool (MaxPooling2D)	(7, 7, 512)	0
flatten (Flatten)	(None, 25088)	0
dense (Dense)	(None, 5)	125445
Total Parameter		20149829

The first block layer has 64 filters with a kernel size of 3x3. The second block has 128 filters with a kernel size of 3x3, the third block 256, and the fourth block 512. The fifth block of the same hyperparameter is performed with a

learning rate of 0.001. Three full connection layers, 4096, 4096, and 1000 were created to apply weights to the inputs generated by feature analysis. In the fifth dense layer, the activation function softmax [15] produces the final probability to determine the class in the image. The loss function uses Categorical Cross-entropy, and optimisation uses Adam[16]. With this, the accuracy matrix was produced, as shown in Table 2.

III. RESULTS

This section presents the results of the experiments carried out with the architecture in Fig. 5. The pre-processing stages, i.e., cleaning and optimisation using contrast stretching, resulted in images measuring 224x224 pixels. Then, the data were labelled and normalised into an array divided by 255 as seen on (3). Then, the grayscale image was converted to binary values of 0 and 1 for class indexing (0: Mild COVID, 1: Severe COVID, 2: COVID Normal, 3: Mild Pneumonia, 4: Severe Pneumonia) as seen on Fig. 6. The next process was the classification output supervised by radiologists. The experts assessed the results of classification done by intelligent computing and determined the accuracy percentage.

$$[array]\ ([[237\ 237\ 237],\ \ [100, 100, 100], [43, 43, 43], [22\ 22\ 22], [25\ 25\ 25], [28\ 28\ 28], \tag{2}$$

$$[array]([[[[0.92941176, 0.92941176\ 0.92941176], [0.39215686, 0.39215686, 0.39215686], [0.16862745, 0.16862745, 0.16862745], [0.08627451, 0.08627451, 0.08627451], [0.09803922, 0.09803922, 0.09803922], [0.10980392, 0.10980392, 0.10980392], \tag{3}$$

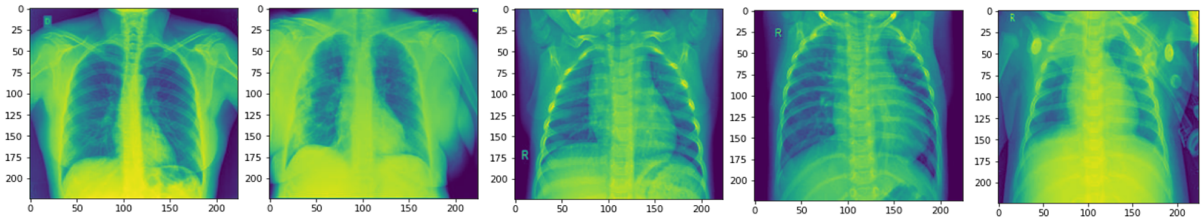

(a) (b) (c)

Fig. 6 The conversion result from chest x-ray (CXR), with images (a) Mild COVID (b) Severe COVID (c) COVID Normal (d) Mild pneumonia (e) Severe pneumonia

This test is divided into three variables: training, testing, and validation for the five classes, as shown in Table 3.

TABLE 3
IMAGE FIVE-CLASSIFIACATION DATASET DISTRIBUTION

Dataset	Training	Testing	Validation
Covid Mild	320	150	150
Covid Severe	320	150	150
Normal	320	150	150
Pneumonia Mild	320	150	150
Pneumonia Severe	320	150	150
Total	**1600**	**750**	**750**

The test results of the five classes with an epoch value of 10 and a batch size of 32 using the VGG 19 model show that, in Mild COVID class, the precision value is 0.98, recall 0.99, F1 score 0.99; in Severe COVID class, the precision value is 0.99, recall 0.98, F1-score 0.99; in Normal class, the precision value is 1.0, recall 0.99, F1-score 1.0. In the Mild Pneumonia class, the precision value is 0.93, recall 1.00, and F1-score 0.96. In the Severe Pneumonia class, the precision value is 1.00, recall 0.94, F1-score 0.97, and an accuracy value of 0.98, as shown in Table 4. In the evaluation matrix, the validation accuracy is presented in Fig. 7 and the validation loss is in Fig. 8. The confusion matrix that is illustrated by Fig. 9 shows the architecture's performance.

TABLE 4
AVERAGE CLASS-WISE PRECISION, RECALL, F1-SCORE OF 5-CLASS

Class	Precision	Recall	F1-Score	Accuracy
Covid Mild	0.98	0.99	0.99	
Covid Severe	0.99	0.98	0.99	
Normal	1.00	0.99	1.00	
Pneumonia Mild	0.93	1.00	0.96	**98%**
Pneumonia Severe	1.00	0.94	0.97	

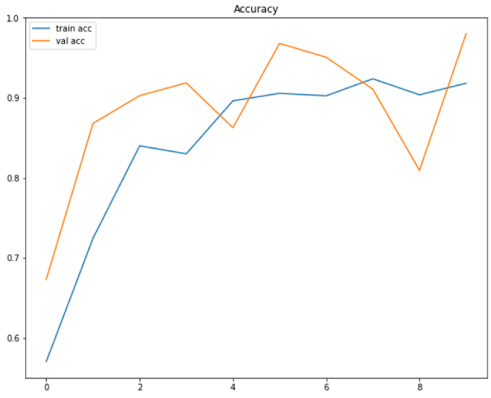

Fig. 7 Validation five class accuracy

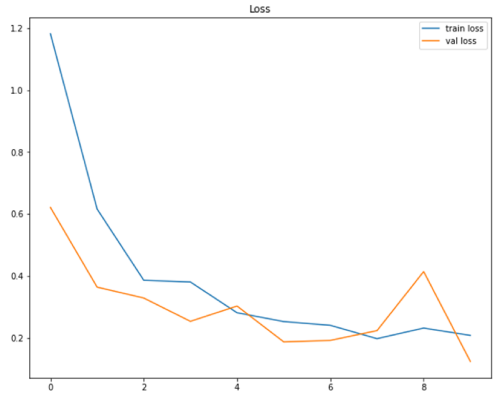

Fig. 8 Validation five class loss

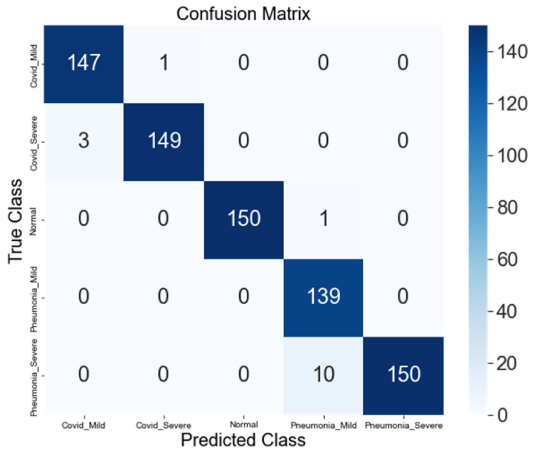

Fig. 9 Predicting matrix (five class)

The test results carried out with three classes are presented in Table 5, showing an epoch value of 10 and a batch size of 32. The test using the VGG 19 in the COVID class resulted in a precision of 1.00, a recall of 0.99, and an F1 score of 1.00; in the Normal class, a precision of 1.00, a recall of 0.99, an F1 score of 1.00; in the Pneumonia class a precision of 0.99, a recall 0.99, and an F1 score of 0.99 with an accuracy of 99.99%. The visual results from the accuracy are presented in Fig. 10. The loss validation is in Fig. 11, and the three-class prediction is presented in Fig. 12.

TABLE 5
AVERAGE CLASS-WISE PRECISION, RECALL, F1-SCORES OF THREE-CLASS PREDICTION

Class	Precision	Recall	F1-Score	Accuracy
Covid-19	1.00	0.99	1.00	
Normal	1.00	0.99	1.00	**99.99%**
Pneumonia	0.99	0.99	0.99	

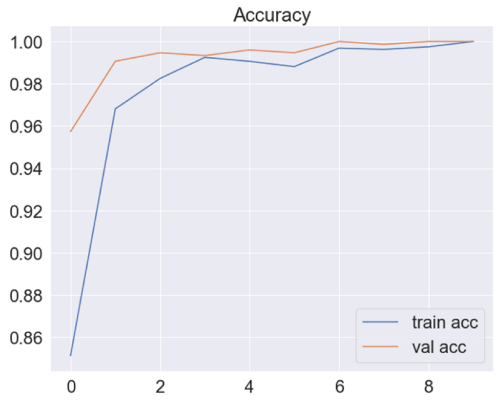

Fig. 10 The three-class validation accuracy

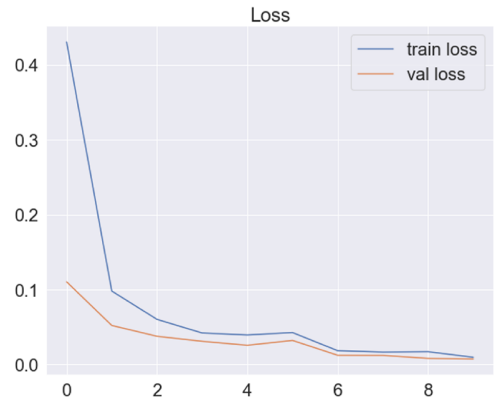

Fig. 11 The three-class validation loss

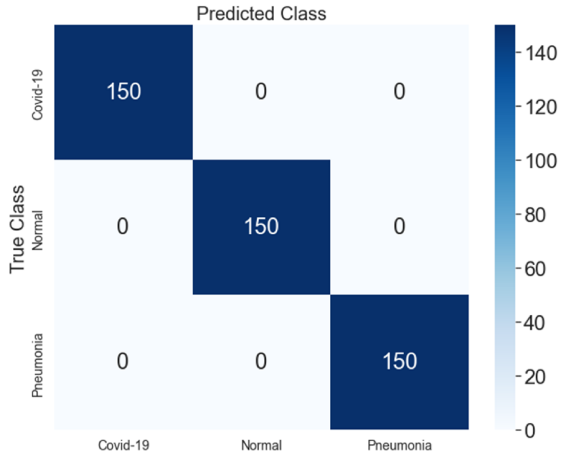

Fig. 12 Validation three-class loss

The test results carried out with two classes are presented in Table 6, with an epoch value of 10 and a batch size of 32. The test using the VGG 19 on the COVID-19 model has a precision value of 1.00, a recall of 0.99, and an F score of 1.00; the Normal class has a precision of 1.00, a recall of 0.99, an F1 score of 1.00, with 99.99% accuracy. The visual representation of the accuracy validation is presented in Fig. 13, and the loss validation in Fig. 14. Meanwhile, the two-class prediction is presented in Fig. 15.

TABLE 6
AVERAGE CLASS-WISE PRECISION, RECALL, F1-SCORE OF THE TWO-CLASS PREDICTION

Class	Precision	Recall	F1-Score	Accuracy
Covid-19	1.00	0.99	1.00	
Normal	1.00	0.99	1.00	**99.99%**

TABLE 7
PERFORMANCES OF FIVE-CLASS, THREE-CLASS AND TWO-CLASS

Class	Precission (%)	Recall (%)	F1-Score (%)	Accuracy (%)
5 Class	0.99	0.99	1.00	98.0
3 Class	1.00	0.99	0.99	99.99
2 Class	1.00	0.99	1.00	99.99

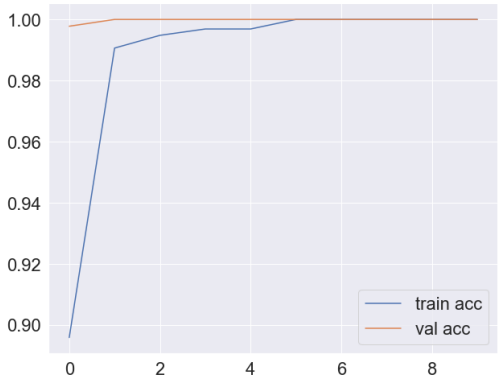

Fig. 13 Validation Two Class Accuracy

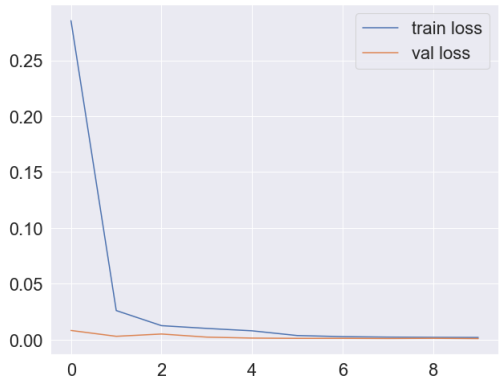

Fig. 14 Validation Two Class Loss

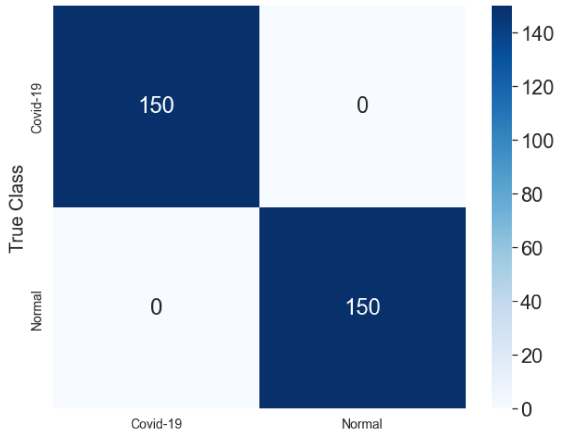

Fig. 15 Validation Three Class Accuracy

From all the tests, the experiments with five classes obtained a precision value of 0.99, a recall of 0.99, an F1 score of 1.00 and an accuracy of 98.0. The experiments with three classes obtained a precision value of 1.00, a recall of 0.99, an F1 score of 1.00 and an accuracy of 99.99%. Meanwhile, in two-class experiments, the precision value was 1.00, recall 0.99, an F1-Score of 1.00 and an accuracy of 99.99%. The test results show an increase in the two-class and the three-class models. However, the five-class model has lower values due to a decrease in performance from the accuracy value, as presented in Fig. 8.

IV. DISCUSSION

We compared the test results in this study with other research methods and results, as shown in Table 8. For example, Apostolopoulos [2] uses the VGG 19 model for testing two-class and three-class predictions with a dataset of 224 COVID+. The results showed 504 in the Normal class and 700 in the Pneumonia class. The accuracy of the two-class is 98.75%, while the accuracy of the three-class is 93.48%. Furthermore, a study by Kedia [17] using the CoVNet-19 model dataset of 1628 COVID+ obtained 2341 Normal and 2345 Pneumonia cases, with an accuracy of 98.28% for the three-class prediction and 99.71% for the two-class. Hemdan [18] used the VGG 19 model on a dataset of 25 COVID+ and 25 COVID- and generated 90% accuracy in the two-class prediction. Gour [19] used the staked CNN model for a three-class prediction, resulting in an accuracy of 92.74%. The study used a dataset of 270 COVID +, which showed 1139 Normal and 1355 Pneumonia. Shelke [20] used the VGG 16 model, Dense-Net 161, and Resnet-18 with a four-class prediction, resulting in an accuracy of 95.9%, 98.9% and 76%, respectively. The study used a dataset of 750 Pneumonia, 1175 COVID-19, 492 Normal, and 382 Tuberculosis. Hussian [21] used the Corodet model and obtained an accuracy of 91.2% (four classes), 94.2% (three classes) and 99.1% (two classes). The datasets used are 500 COVID-19, 400 Normal, 400 Viral Pneumonia, and 800 Bacterial Pneumonia. The proposed model's accuracy for the five-class prediction was 98%, three-class was at 99.99%, and two-class was at 99.99%. However, this study has a limited dataset, and the hardware's ability to test is one of the determining factors.

TABLE 8
PERFORMANCES OF FIVE-CLASS, THREE-CLASS AND TWO-CLASS

Reference Study	Model	5 Classes	4 Classes	3 Classes	2 Classes	Image
Ioannis	VGG 19	N/A	N/A	93.48%	98.75%	224COVID+ 504 Normal 700Pneumonia
Piyanh Kedia	CoVNet-19	N/A	N/A	98.28%	99.71%	1628 COVID+ 2341 Normal 2345 Pneumonia
Hemdan	VGG 19	N/A	N/A	N/A	90.0%	25 COVID+ 25 COVID-
M. Gour	Staked CNN	N/A	N/A	92.74%	N/A	270 COVID+ 1139 Normal 1355Pneumonia
A. Shelke	VGG 16, DenseNet-161 Resnet-18	N/A	95.9% 98.9% 76%	N/A	N/A	750Pneumonia 1175COVID-19 492 Normal 382Tubercolosis
Emtiaz Hussian	CoroDet	N/A	91.2%	94.2%	99.1%	500 COVID-19 400 Normal 400 Pneumonia Viral 800 Pneumonia Bacterial
Proposed Method	**VGG 19**	**98%**	**N/A**	**99.99%**	**99.99%**	**470 COVID Mild** **470 COVID Severe** **470 Normal** **470 Pneumonia Mild** **470 Pneumonia Severe**

V. CONCLUSIONS

The experiments show that the VGG 19 model can produce an accuracy of 98% in the five new classes (Severe COVID, Mild COVID, Normal, Severe pneumonia, and Mild pneumonia). The three-class and two-class predictions' accuracy compares the proposed model's performance. This study achieved 99.99% for both three classes and two classes. This accuracy result was achieved by avoiding cross-validation on the dataset.

Author Contributions: *Endra Yuliawan*: Conceptualisation, Methodology, Software, Writing - Original Draft. *Softwatul 'Uyun*: Writing - Review, Supervision, Validation

Funding: This research received no specific grant from any funding agency.

Acknowledgements: We would like to thank dr. Ita Rima Rahmawati, Sp.Rad(K) for the assistance in classifying the chest X-ray dataset and consultancy.

Conflicts of Interest: The authors declare no conflict of interest.

REFERENCES

[1] Y. Chen, Q. Liu, and D. Guo, "Emerging coronaviruses : Genome structure , replication , and pathogenesis," no. January, pp. 418–423, 2020, doi: 10.1002/jmv.25681.

[2] I. D. Apostolopoulos and T. A. Mpesiana, "Covid-19: automatic detection from X-ray images utilizing transfer learning with convolutional neural networks," *Phys. Eng. Sci. Med.*, vol. 43, no. 2, pp. 635–640, 2020, doi: 10.1007/s13246-020-00865-4.

[3] J. F. W. Chan *et al.*, "A familial cluster of pneumonia associated with the 2019 novel coronavirus indicating person-to-person transmission: a study of a family cluster," *Lancet*, vol. 395, no. 10223, pp. 514–523, 2020, doi: 10.1016/S0140-6736(20)30154-9.

[4] S. A. Lauer *et al.*, "The incubation period of coronavirus disease 2019 (CoVID-19) from publicly reported confirmed cases: Estimation and application," *Ann. Intern. Med.*, vol. 172, no. 9, pp. 577–582, 2020, doi: 10.7326/M20-0504.

[5] J. Liu *et al.*, "Community Transmission of Severe Acute Respiratory," *Emerg. Infect. Dis.*, vol. 26, no. 6, pp. 1320–1323, 2020.

[6] World Health Organization, "Infection Prevention and Control of Epidemic-and Pandemic-prone Acute Respiratory Infections in Health Care," *Infect. Prev. Control Epidemic-and Pandemic-prone Acute Respir. Infect. Heal. Care*, vol. 2, no. 12, p. 7, 2014.

[7] B. van G. and R. M. S. H. Greenspan, "Guest Editorial Deep Learning in Medical Imaging : Overview and Future Promise of an Exciting New Technique," vol. 35, no. 5, pp. 1153–1159, 2016, doi: 10.1109/TMI.2016.2553401.

[8] L. Deng, O. M. Way, D. Yu, and O. M. Way, "Deep Learning : Methods and Applications".

[9] A. I. Khan, J. L. Shah, and M. M. Bhat, "CoroNet: A deep neural network for detection and diagnosis of COVID-19 from chest x-ray images," *Comput. Methods Programs Biomed.*, vol. 196, p. 105581, 2020, doi: 10.1016/j.cmpb.2020.105581.

[10] D. S. Kermany *et al.*, "Identifying Medical Diagnoses and TreaTable Diseases by Image-Based Deep Learning," *Cell*, vol. 172, no. 5, pp. 1122-1131.e9, 2018, doi: 10.1016/j.cell.2018.02.010.

[11] N. Wakhidah, "Perbaikan Kualitas Citra Menggunakan Metode Contrast Stretching," *J. Transform.*, vol. 8, no. 2, p. 78, 2011, doi: 10.26623/transformatika.v8i2.48.

[12] K. Simonyan and A. Zisserman, "Very deep convolutional networks for large-scale image recognition," *3rd Int. Conf. Learn. Represent. ICLR 2015 - Conf. Track Proc.*, pp. 1–14, 2015.

[13] T. F. Gonzalez, "Handbook of approximation algorithms and metaheuristics," *Handb. Approx. Algorithms Metaheuristics*, pp. 1–1432, 2007, doi: 10.1201/9781420010749.

[14] S. Joseph, "Australian Literary Journalism and 'Missing Voices': How Helen Garner finally resolves this recurring ethical tension," *Journal. Pract.*, vol. 10, no. 6, pp. 730–743, 2016, doi: 10.1080/17512786.2015.1058180.

[15] Y. Lecun, Y. Bengio, and G. Hinton, "Deep learning," *Nature*, vol. 521, no. 7553, pp. 436–444, 2015, doi: 10.1038/nature14539.

[16] D. P. Kingma and J. L. Ba, "Adam: A method for stochastic optimization," *3rd Int. Conf. Learn. Represent. ICLR 2015 - Conf. Track Proc.*, pp. 1–15, 2015.

[17] P. Kedia, Anjum, and R. Katarya, "CoVNet-19: A Deep Learning model for the detection and analysis of COVID-19 patients," *Appl. Soft Comput.*, vol. 104, p. 107184, 2021, doi: 10.1016/j.asoc.2021.107184.

[18] E. E.-D. Hemdan, M. A. Shouman, and M. E. Karar, "COVIDX-Net: A Framework of Deep Learning Classifiers to Diagnose COVID-19 in X-Ray Images," 2020, [Online]. Available: http://arxiv.org/abs/2003.11055

[19] M. Gour and S. Jain, "Stacked Convolutional Neural Network for Diagnosis of COVID-19 Disease from X-ray Images," 2020, [Online]. Available: http://arxiv.org/abs/2006.13817

[20] A. Shelke *et al.*, "Chest X-ray Classification Using Deep Learning for Automated COVID-19 Screening," *SN Comput. Sci.*, vol. 2, no. 4, pp. 1–9, 2021, doi: 10.1007/s42979-021-00695-5.

[21] E. Hussain, M. Hasan, M. A. Rahman, I. Lee, T. Tamanna, and M. Z. Parvez, "CoroDet: A deep learning based classification for COVID-19 detection using chest X-ray images," *Chaos, Solitons and Fractals*, vol. 142, p. 110495, 2021, doi: 10.1016/j.chaos.2020.110495.